Pergamon

0301-9322(93)E0020-6

Int. J. Multiphase Flow Vol. 20, No. 3, pp. 579–591, 1994

0301-9322/94 $7.00 + 0.00

VISCOUS RESUSPENSION IN FULLY DEVELOPED LAMINAR PIPE FLOWS

K. ZHANG and A. ACRIVOS
The Levich Institute, The City College of CUNY, New York, NY 10031, U.S.A.

(Received 25 August 1993; in revised form 11 November 1993)

Abstract—Viscous resuspension of heavy particles in fully developed laminar flows in a horizontal pipe is investigated theoretically by extending the model used previously for unidirectional flows to cases in which all three velocity components are non-zero due to the existence of a secondary motion within the cross section of the pipe. The resulting mathematical system of equations was solved by employing the Galerkin finite-element method. The theoretically predicted velocity and concentration profiles for flow in a circular pipe were found to be in very good qualitative agreement with experimental results reported by others, even though the analysis did not make use of any adjustable parameters.

Key Words: resuspension, pipe flow

1. INTRODUCTION

It was reported in earlier publications (c.f. Leighton & Acrivos 1987) that, in concentrated suspensions undergoing shear, a flux of particles is induced from regions of high shear to low and from regions of high particle concentrations to low. This phenomenon, termed shear-induced diffusion, arises from the hydrodynamic interaction among neighboring particles and often creates a non-uniform particle distribution in flowing suspensions that were initially well mixed. This fact has important implications in the field of viscometry where the interpretation of effective viscosity measurements in concentrated suspensions is subject to serious errors if the shear-induced non-uniformity in the particle concentration within the measuring device is not properly taken into account. It is also an important factor in many industrial processes of material manufacturing, where the performance of the finished product is greatly affected by the degree of solids dispersivity (Sinton & Chow 1991). In addition, shear-induced particle diffusion is responsible for the observed phenomenon of viscous resuspension wherein, under the action of shear, an initially settled bed of particles in contact with a clear fluid above it can be resuspended and the particles kept in suspension even under laminar flow conditions (Leighton & Acrivos 1986; Acrivos *et al.* 1993).

To date, shear-induced diffusion and viscous resuspension have been investigated theoretically only for a few unidirectional or quasi-unidirectional flows, e.g. Couette flow, channel flow and flow down an inclined plate (Leighton & Acrivos 1986, 1987; Schaflinger *et al.* 1990; Nir & Acrivos 1990; Phillips *et al.* 1992; Koh *et al.* 1994; Acrivos *et al.* 1993), but not for any of the numerous multidimensional flows which are more often encountered in practice. One such example is the flow in a horizontal circular pipe of an initially well-mixed suspension of heavy particles in a viscous fluid which, far from the entrance, becomes stratified with the suspension occupying the bottom portion of the pipe and the clear fluid above it. Here, in contrast to the corresponding suspension flow of neutrally buoyant particles (Phillips *et al.* 1992), the existence of a non-axisymmetric density distribution induces a secondary flow within the cross-section of the pipe and, hence, even for a fully-developed flow, all three velocity components will be non-zero and will be functions of the two transverse coordinates. Obviously, this secondary flow generates a convective particle flux along the cross-sectional plane, in addition to the flux due to shear-induced diffusion and gravitational sedimentation. Such secondary flow patterns also are created when a suspension of heavy particles is made to flow in a channel when the side-wall effects cannot be ignored, as well as in a wide-gap Couette viscometer.

The purpose of this paper is to present a theoretical analysis of a class of these more complicated resuspension flows. In the next section, we develop a mathematical model, essentially identical to

that used previously (Schaflinger *et al.* 1990), in which the suspension is viewed as an effective continuum Newtonian fluid with concentration-dependent effective properties. This model, which also includes the contribution of shear-induced particle diffusion due to gradients both in the concentration and in the shear, leads to a system of 5 partial differential equations in the two transverse coordinates, i.e. the continuity equation, the 3 momentum equations and the balance equation for the solid particles, rather than 2 ordinary differential equations as for a unidirectional flow (Schaflinger *et al.* 1990). These equations are strongly coupled and non-linear and their solution is stiff, in the sense that, as the suspension–clear fluid interface, the location of which is unknown *a priori*, is approached from below, the particle concentration varies rapidly over a small distance. A special numerical code was therefore developed using the Galerkin finite-element method. The numerical algorithms adopted in the code will be described in section 3.

The fully developed suspension flow within a horizontal circular pipe was then examined on the basis of this code, and the numerical results thereby obtained, which did not entail the use of any adjustable parameters, will be compared in section 4 with the experimental results reported by Altobelli *et al.* (1991), who measured the corresponding flow velocities and particle distributions by employing the technique of nuclear magnetic resonance imaging. These are, to our knowledge, the only comparable measurements for a non-unidirectional suspension flow. Some of these experimental results are especially interesting and rather surprising, e.g. the observation that, for the case of a large mean particle concentration, a highly concentrated core formed slightly above the pipe centerline. It will be seen that our theoretical predictions are in very good qualitative agreement with all the experimental findings referred to above.

2. MATHEMATICAL FORMULATION

Consider then the flow of a suspension of heavy solid spherical particles of radius a in a liquid of viscosity μ_1 when the mixture can be modeled as an effective continuum Newtonian fluid with concentration-dependent effective properties. We further suppose that the particle Reynolds number is vanishingly small. The equations of motion for the suspension reduce therefore to the incompressible Navier–Stokes equations in terms of bulk-averaged effective quantities, such as the velocity $\mathbf{u}$ and

$$\rho = 1 + \epsilon\Phi, \quad \text{with} \quad \epsilon = \frac{\rho_2 - \rho_1}{\rho_1} \geqslant 0, \tag{1}$$

where ρ is the effective density divided by ρ_1, the density of the pure fluid, ρ_2 is the density of the particles and Φ is their volume fraction. The effective viscosity of the suspension on the other hand can be represented by a large variety of empirical correlations, among which those used in previous analyses of unidirectional flows are

$$\mu = \left(1 - \frac{\Phi}{\Phi_m}\right)^{-1.82}, \tag{2}$$

given by Krieger (1972), and

$$\mu = \left(1 + \frac{1.5\Phi}{1 - \dfrac{\Phi}{\Phi_m}}\right)^2, \tag{3}$$

proposed by Leighton & Acrivos (1987). Here, μ is the suspension viscosity divided by μ_1, and Φ_m is the solid volume fraction beyond which the suspension can no longer flow. As in our previous studies (Leighton & Acrivos 1986; Schaflinger *et al.* 1990) we shall set $\Phi_m = 0.58$.

The particle conservation equation is obtained by balancing the fluxes due to bulk convection, gravitational sedimentation and shear-induced diffusion and by neglecting Brownian diffusion.

Next, following a standard approach, we set the settling velocity of a test sphere in the suspension, relative to the bulk velocity, equal to the product of the Stokes settling velocity of an isolated sphere times a monotonically decreasing function of Φ, the so-called hindrance function $f(\Phi)$, which accounts for the reduction in the settling velocity due to particle interactions. Thus, the expression for the sedimentation flux becomes

$$\mathbf{N}_G = \frac{2}{9}\frac{a^2(\rho_2 - \rho_1)}{\mu_1}\Phi f(\Phi)\mathbf{g}, \qquad [4]$$

where, as done previously (Leighton & Acrivos 1986; Schaflinger *et al.* 1990), we approximate $f(\Phi)$ by means of

$$f \cong \frac{1-\Phi}{\mu}. \qquad [5]$$

As mentioned earlier, up to now, expressions for the flux due to shear-induced particle diffusion have been proposed and tested experimentally only for unidirectional flows in which both the shear and the particle volume fraction are functions of a single position variable. Thus, for example, according to Leighton & Acrivos (1987), the particle flux can be expressed as

$$\mathbf{N}_d = -D_c\nabla\Phi - D_s\nabla\dot{\gamma}, \qquad [6]$$

where the scalars D_c and D_s are, respectively, shear-induced diffusion coefficients and $\dot{\gamma}$ is the shear rate. In general, however, one would expect the expression for the particle flux to be more complicated and the diffusion coefficients to be second-order tensors rather than scalars. Indeed, as shown by Leighton & Acrivos (1987), even in unidirectional flows the coefficient multiplying the concentration gradient in [6] has a different value depending on whether the diffusion is normal to the plane of shear or parallel to it. Nevertheless, in order to keep the analysis as simple as possible, we shall proceed with our model by generalizing [6] and retaining D_c and D_s as scalars. In addition, we let the effective shear rate $\dot{\gamma}$ in [6] be proportional to the square root of the second invariant of the rate of deformation tensor $\mathbf{d}$, i.e.

$$\dot{\gamma} = (2\mathbf{d}:\mathbf{d})^{1/2}, \qquad [7]$$

where $\mathbf{d} \equiv \frac{1}{2}(\nabla\mathbf{u} + \nabla\mathbf{u}^T)$. For unidirectional flows, $\dot{\gamma}$ in [7] is equal to the absolute value of the component of the shear-rate tensor along the direction of principal shear.

Based on dimensional analysis and the mechanisms of shear-induced diffusion, it was found (Leighton & Acrivos 1987) that the coefficient D_c should be proportional to $a^2\dot{\gamma}$, while D_s should be proportional to a^2. The dimensionless forms of these coefficients, which were used in previous analyses of unidirectional suspension flows, are:

$$\hat{D}_c \equiv \frac{D_c}{a^2\dot{\gamma}} = 0.43\Phi + 0.65\Phi^2\frac{1}{\mu}\frac{d\mu}{d\Phi}, \quad \hat{D}_s \equiv \frac{D_s}{a^2} = 0.43\Phi^2, \qquad [8]$$

with [2] for μ (Phillips *et al.* 1992); and

$$\hat{D}_c = \tfrac{1}{3}\Phi^2(1 + \tfrac{1}{2}e^{8.8\Phi}) + 0.6\Phi^2\frac{1}{\mu}\frac{d\mu}{d\Phi}, \quad \hat{D}_s = 0.6\Phi^2, \qquad [9]$$

with [3] for μ (Leighton & Acrivos 1987; Schaflinger *et al.* 1990; Acrivos *et al.* 1993).

We now restrict our attention to fully developed flows in horizontal pipes, which are driven either by pressure (Poiseuille flows) or by a boundary motion (Couette flows). These flows are two-dimensional, in the sense that the flow velocity and the particle concentration vary only along the cross section of the pipes. Let us further denote by x_1 and x_2 the coordinates along, respectively, the horizontal and vertical directions within the cross section. Then, by introducing L and U,

respectively, as the characteristic length and velocity, we can write the governing equations in dimensionless form:

$$\frac{\partial u_j}{\partial x_j} = 0, \tag{10}$$

$$\mathrm{Re}(1+\epsilon\Phi)\left(\frac{\partial u_i}{\partial t} + u_j\frac{\partial u_i}{\partial x_j}\right) = \frac{\partial}{\partial x_j}[-p\delta_{ij} + 2\mu(\Phi)d_{ij}] - \frac{1}{\mathrm{Fr}}\Phi\delta_{i2}, \quad i = 1, 2, \tag{11}$$

$$\mathrm{Re}(1+\epsilon\Phi)\left(\frac{\partial u_3}{\partial t} + u_j\frac{\partial u_3}{\partial x_j}\right) = K + \frac{\partial}{\partial x_j}(2\mu(\Phi)d_{3j}), \tag{12}$$

and

$$\frac{\partial\Phi}{\partial t} + u_j\frac{\partial\Phi}{\partial x_j} = \lambda\frac{\partial}{\partial x_j}\left[\hat{D}_c(\Phi)\dot{\gamma}\frac{\partial\Phi}{\partial x_j} + \hat{D}_s(\Phi)\frac{\partial\dot{\gamma}}{\partial x_j} + \frac{2}{9\,\mathrm{Fr}}\Phi f(\Phi)\delta_{j2}\right], \tag{13}$$

where (and hereafter) the summation convention for repeated indices ($j = 1, 2$) is used and δ_{ij} is the Kronecker delta. This system of equations contains 4 control parameters: the Reynolds number $\mathrm{Re} \equiv \rho_1 UL/\mu_1$, based on the properties of the suspending fluid; the modified Froude number $\mathrm{Fr} \equiv \mu_1 U/(\rho_2 - \rho_1)gL^2$; the relative density ratio of the suspended particles to the suspending fluid $\epsilon \equiv (\rho_2 - \rho_1)/\rho_1$; and, $\lambda \equiv (a/L)^2$, the square of the ratio of the particle size to the characteristic length scale. The symbol K in [12] refers to the dimensionless pressure drop per unit length along the length of the pipe in Poiseuille flows. For Couette flows, $K = 0$.

To complete the formulation, we now turn to the boundary conditions. Although there is ample evidence for the existence in suspension flows of a relative velocity along the solid walls, especially when the suspension is concentrated (Yilmazer & Kalyon 1989), sample calculations for the simpler case of fully developed flow in a channel treated earlier (Schaflinger *et al.* 1990) showed that the addition of a relative velocity had a minor effect on the pressure drop and the height of the resuspended region for any given set of parameters, hence here we consider only the case of no slip. In addition, we require that the particle flux into a boundary be equal to zero, i.e. that

$$(\mathbf{N}_G + \mathbf{N}_d)_j\mathbf{n}_j = 0, \quad j = 1, 2, \tag{14}$$

where $\mathbf{n}_j$ is the unit normal to each boundary. This zero flux condition applies not only on solid walls but also on surfaces of symmetry. Finally, if transient solutions are required, then obviously initial conditions need to be given.

3. NUMERICAL METHODS

The system of equations [10]–[13] differs in two respects from that which applies typically in pure fluids. First, the diffusion coefficient D_c depends not only on the scalar Φ but also on the effective shear rate $\dot{\gamma}$ and, furthermore, there is an additional diffusive term, i.e. the second term on the right-hand side of [13], which involves third-order derivatives of the flow velocity. Secondly, as seen from [2] and [3] and [8] and [9], the viscosity and the diffusion coefficients are all highly non-linear functions of Φ. To numerically solve this coupled system of non-linear equations, we chose to use the Galerkin finite-element method.

Since the Re values for laminar suspension flows are typically low or moderate, we adopt the penalty formulation (c.f. Baker 1983) for [10] and [11] of the secondary flow. In this formulation, the suspension is supposed to be slightly compressible, and then the pressure is defined by

$$p = -\alpha_n\,\mathrm{Re}\,\mu\frac{\partial u_j}{\partial x_j}, \tag{15}$$

with the penalty parameter α_n being a large positive constant (Hughes *et al.* 1979). The pressure, therefore, is no longer a primary field variable. This is important for reducing the computational requirements, especially if one desires to extend the present numercial analysis to fully three-

dimensional suspension flows. Now, substituting [15] into [11], multiplying [11] by a weighting function w and then integrating over the cross section Ω, we obtain the weak form of [11]:

$$\int_\Omega w(1+\epsilon\Phi)\left(\frac{\partial u_i}{\partial t}+u_j\frac{\partial u_i}{\partial x_j}\right)\mathrm{d}x+\frac{1}{\mathrm{Re}}\int_\Omega \mu\frac{\partial w}{\partial x_j}\left(\frac{\partial u_i}{\partial x_j}+\frac{\partial u_j}{\partial x_i}\right)\mathrm{d}x + \alpha_n\int_\Omega \mu\frac{\partial w}{\partial x_i}\frac{\partial u_j}{\partial x_j}\mathrm{d}x=-\frac{1}{\mathrm{Re\,Fr}}\int_\Omega w\Phi\delta_{i2}\,\mathrm{d}x,\quad i,j=1,2, \quad [16]$$

where the divergence theorem has been used. Similarly, for [12], we have:

$$\int_\Omega w(1+\epsilon\Phi)\left(\frac{\partial u_3}{\partial t}+u_j\frac{\partial u_3}{\partial x_j}\right)\mathrm{d}x+\frac{1}{\mathrm{Re}}\int_\Omega \mu\frac{\partial w}{\partial x_j}\frac{\partial u_3}{\partial x_j}\mathrm{d}x=\frac{K}{\mathrm{Re}}\int_\Omega w\,\mathrm{d}x. \quad [17]$$

We require that the weighting function w in [16] and [17] vanishes on that portion of the boundary where the velocity is prescribed.

As stated in the introduction, the solution of [13] may vary sharply within a thin layer adjacent to the suspension–clear fluid interface. In addition, the location of this interface, which is moving in a time-dependent simulation, must be found as part of the solution. Therefore, it seems that an efficient way of constructing these solutions would be to track the interface explicitly and use an adaptive mesh. Nevertheless, because the implementation of such a method would be too complicated, we chose to solve [13] using a fixed mesh over the whole domain Ω, even though this might significantly increase the computational requirements. Thus, multiplying [13] by a weighting function W and integrating over Ω, we have

$$\int_\Omega W\left(\frac{\partial\Phi}{\partial t}+u_j\frac{\partial\Phi}{\partial x_j}\right)\mathrm{d}x+\lambda\int_\Omega\frac{\partial W}{\partial x_j}\left[\hat{D}_c(\Phi)\dot{\gamma}\frac{\partial\Phi}{\partial x_j}+\hat{D}_s(\Phi)\frac{\partial\dot{\gamma}}{\partial x_j}+\frac{2}{9\,\mathrm{Fr}}\Phi f(\Phi)\delta_{j2}\right]\mathrm{d}x=0, \quad [18]$$

where the boundary condition [14] has been applied.

The weighting functions we used in [16]–[18] are the same as the shape functions. However, as is well-known, in solving convection–diffusion equations by this conventional Galerkin finite-element method, the solutions may exhibit numerical oscillations whenever the finite-element mesh is not fine enough to model sharp variations in these solutions. In fact, we obtained some solutions in which the concentration Φ oscillated, particularly, about the value $\Phi=0$ in the region of the clear fluid. Dealing with such a numerical instability has been an active area of research in the finite-element field and many techniques, such as the streamline-upwind/Petrov–Galerkin method (Brooks & Hughes 1982) and the Taylor–Galerkin method (Usmani *et al.* 1992) have been suggested. As yet, we have not applied these techniques to improve the quality of our solutions.

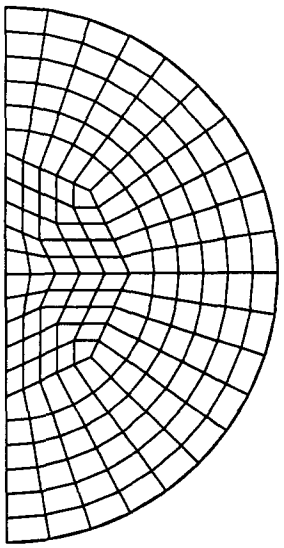

Figure 1. Finite-element mesh with 170 elements, 9 element nodes and 723 global nodes.

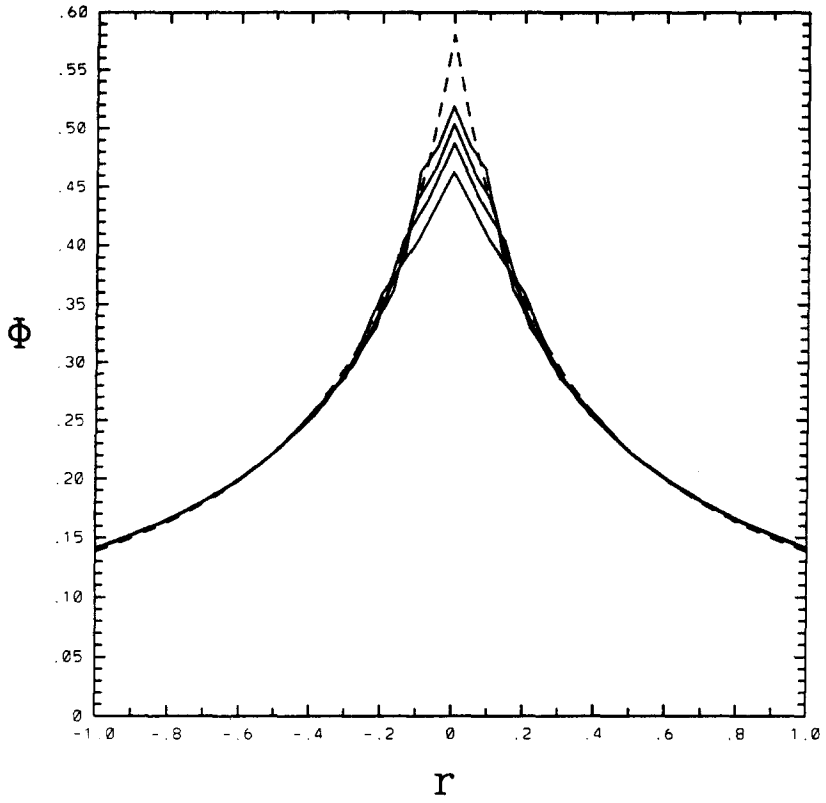

Figure 2. The axisymmetric concentration profiles Φ for $\epsilon = 0$ and $\bar{\Phi} = 0.2$. The dashed curve represents the analytical solution given by Phillips *et al.* (1992) and the solid curves are the numerical solutions using, respectively, 32, 66, 112 and 170 elements.

Instead, we used a simple filtering procedure to remove such numerical noise in Φ, which occured in the region of the clear fluid, by setting $\Phi = 0$ if its computed value was less than a preset constant $0 < C \ll 1$, typically equal to 2×10^{-3}. The actual value chosen for C was adjusted to ensure maximal conservation of the total volume of solid particles within the cross section, i.e. $\int_\Omega \Phi \, dx$.

In the spatial discretization of [16]–[18] we used the isoparametric, quadrilateral, Lagrangian quadratic elements (c.f. Reddy 1984). Thus, the dependent variables in [16]–[18] were interpolated in terms of the quadratic shape functions ψ_k, i.e.

$$u_i = \psi_k U_{ik}, \quad \Phi = \psi_k \Phi_k, \quad i = 1, 2, 3, \qquad [19]$$

where U_{ik} and Φ_k denote the values of, respectively, the velocity components and the concentration at the nodal point k. Then, these interpolations were substituted into [16]–[18], and the resulting integrals were calculated by means of a second-order Gaussian quadrature. However, a first-order quadrature was used in evaluating the penalty term in [16] in order to maintain numerical stability. Moreover, in the integrations, the function $1 + \epsilon\Phi$ was taken as constant within each element and equal to its value at the center node of the element.

We found in our simulations that computational accuracy in the effective shear rate $\dot{\gamma}$ was essential for obtaining accurate solutions. Accordingly, we defined $\dot{\gamma}$ as a primary variable and computed it from the algebraic equation [7]. We tried several techniques which have been used in computing the vorticity and the pressure from finite-element solutions of the velocity (Lee *et al.* 1979), and found that a local smoothing scheme gave the best results. This scheme consists of three steps. First, the components of the shear-rate tensor $\mathbf{d}$ and its second invariant $\dot{\gamma}$ are calculated at the element Gaussian points using

$$d_{ij} = \frac{1}{2}\left(\frac{\partial \psi_k}{\partial x_i} U_{jk} + \frac{\partial \psi_k}{\partial x_j} U_{ik}\right) \qquad [20]$$

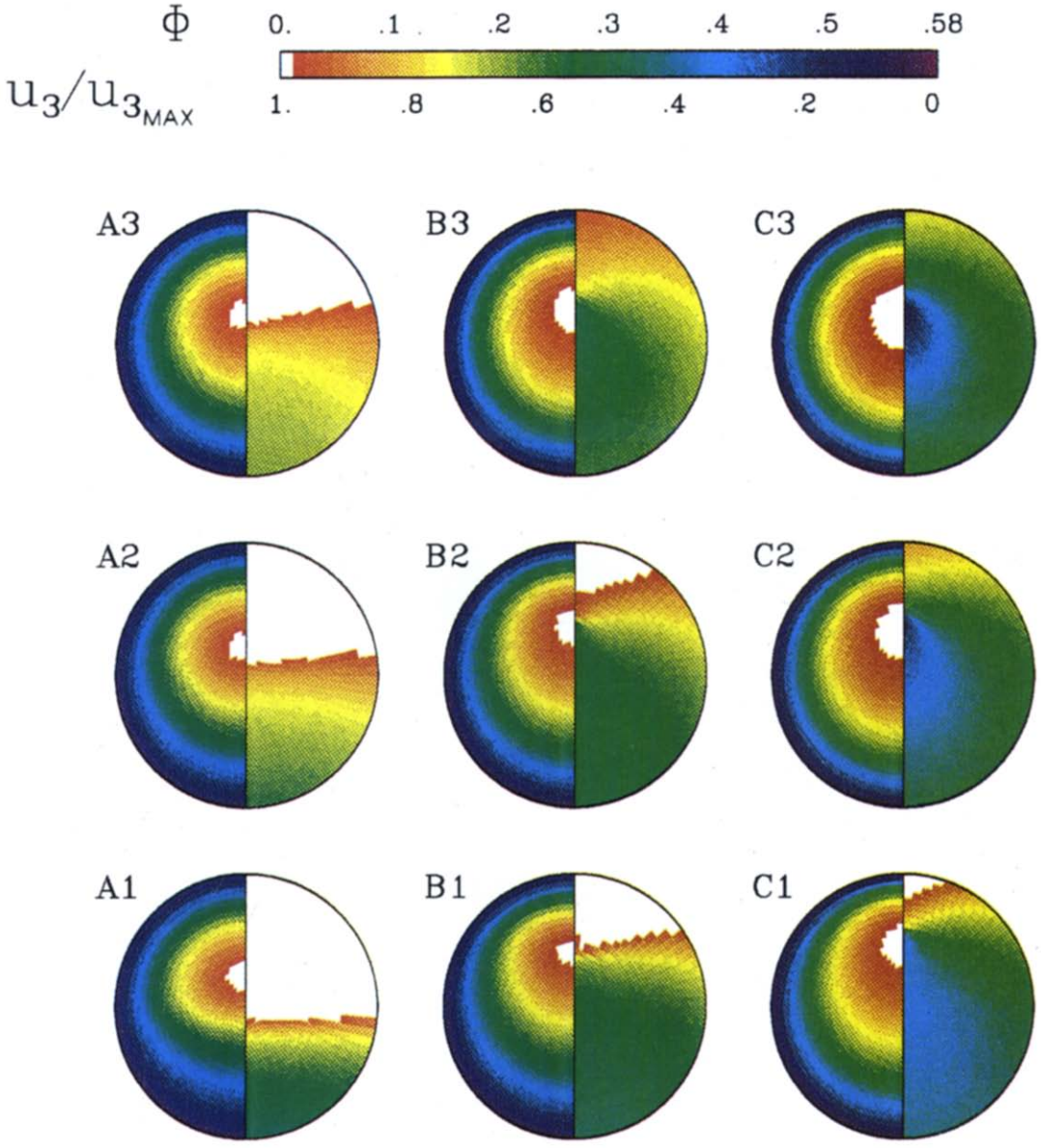

Figure 3. The contours of concentration Φ (on the right half circle) and the normalized axial velocity $u_3/u_{3\max}$ (on the left half circle) for $\epsilon = 0.2$ and $\lambda = 10^{-3}$. The columns A, B and C correspond to, respectively, $\bar{\Phi} = 0.1$, 0.2 and 0.3, while the rows 1, 2 and 3 correspond to (Re, Fr) = (5, 0.25), (10, 0.5) and (20, 1).

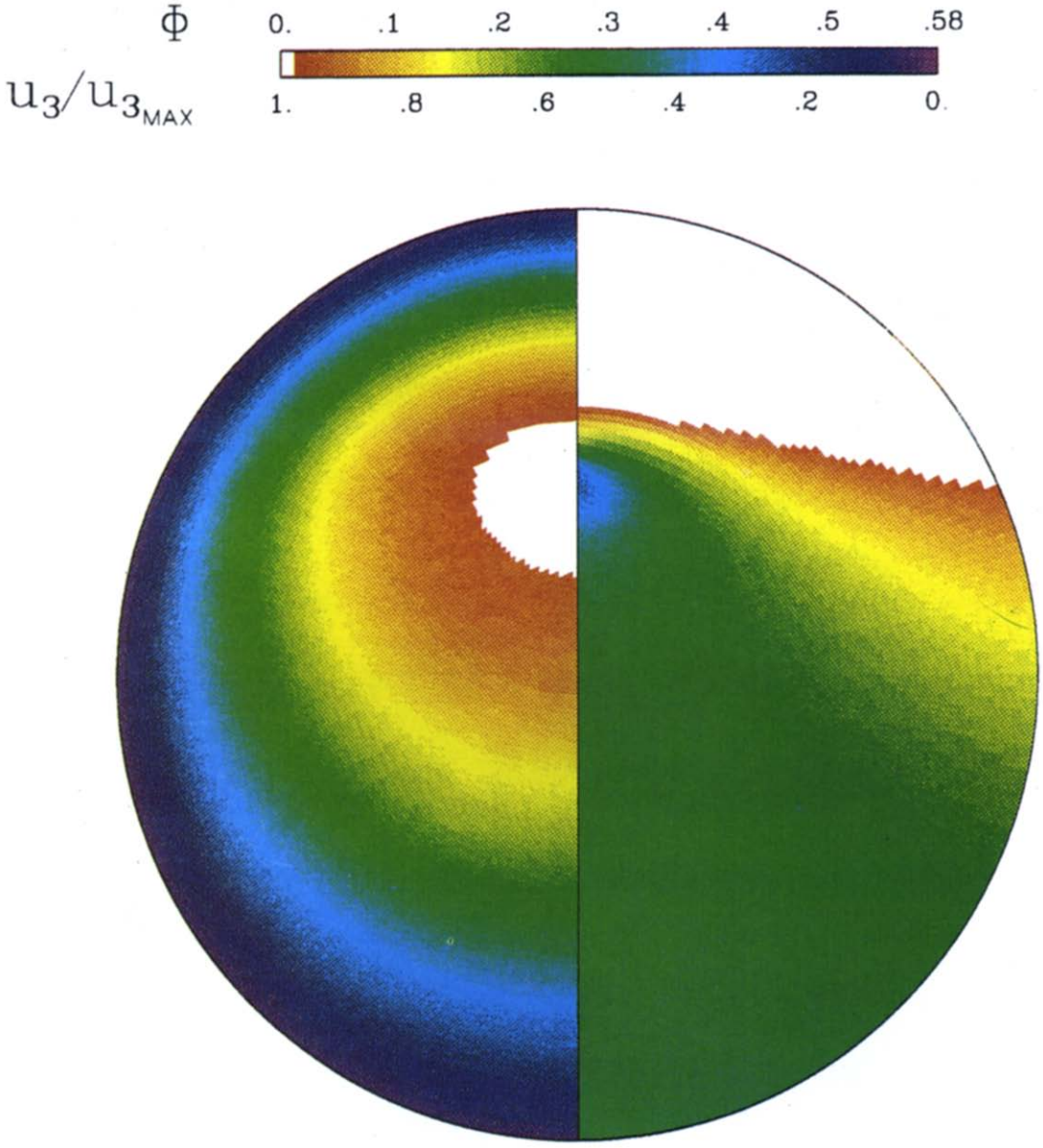

Figure 6. The contours of the concentration Φ (on the right half circle) and the normalized axial velocity $u_3/u_{3\max}$ (on the left half circle) for case B1 in figure 3 but without the secondary-flow convection.

and [7], and then the values of $\dot{\gamma}$ at the nodes of each element are obtained by linear extrapolations. Finally, those node values arising from elements which join at a given (global) node are everged to give a unique value of $\dot{\gamma}$ at that node.

All of our numerical computations were time-dependent and, whenever a steady solution was required, it was obtained as the time-asymptotic result of transient solutions. This approach allowed us to decouple and linearize [16]–[18] by means of successive substitutions in a time-stepping procedure. Specifically, this procedure entailed the following steps:

1. It was assumed that all the dependent variables were known at time step t_n.
2. The concentration Φ was calculated at time t_{n+1} from [18], using values of all the variables and of the diffusion coefficients at time t_n.
3. The velocity components u_1 and u_2 of the secondary flow were calculated from [16], using the updated values of Φ obtained in Step 2.
4. The axial velocity u_3 was calculated from [17], using the updated values of Φ, u_1 and u_2 obtained in Steps 2 and 3.
5. The effective shear rate $\dot{\gamma}$ was calculated from [7] and [20], using all of the updated values.
6. The process was then begun anew starting from Step 1.

In addition, the diffusive terms and the penalty term in [16]–[18] were treated implicitly, except for the term $\hat{D}_s(\Phi)\partial\dot{\gamma}/\partial x_j$ in [18], which became an explicit force term in the implementation of the above procedure. On the other hand, the convective terms in [16]–[18] were treated explicitly. In this way, the resulting system of linear algebraic equations was banded and symmetric, and was solved by Gaussian eliminations and back substitutions. The explicit evaluation of the convective terms imposes a stability limitation on the time step size, Δt, which was kept constant for most of our computations.

4. THE STEADY FLOW WITHIN A CIRCULAR PIPE

Based on the algorithms described in the last section, we developed a finite-element code and then applied it to the fully developed, pressure-driven, steady suspension flow within a circular pipe. For this flow, we chose as the characteristic length and velocity, respectively, the radius of the pipe, R, and Q/R^2, where Q is the volumetric flow rate. Then, the pressure gradient K in [12] was determined by the flow-rate equation, i.e.

$$\int_\Omega u_3 \, dx = 1, \qquad [21]$$

with the domain of integration Ω extending over the entire cross-sectional area. In addition, because the vertical diameter of the circular cross section is now a symmetric surface, solutions over only half of the circle are needed. Figure 1 shows the finite-element mesh used for most of the results given hereafter. During the construction of this mesh, every effort was made to reduce distortion of the elements.

We computed the steady solutions, as mentioned earlier, as time-asymptotic results of time-dependent solutions, and used as initial conditions the parabolic velocity profile of a single-phase fluid and a uniform concentration $\bar{\Phi}$. Because, as can be seen from [13], the mean concentration within the cross section, i.e.

$$\bar{\Phi} = \frac{1}{\Omega}\int_\Omega \Phi \, dx, \qquad [22]$$

must remain unchanged at any time step, we used this condition as one of the tests of computational accuracy in our simulations. In fact, in all of our simulations, $\bar{\Phi}$ remained unchanged to at least one part in 10^6 up to the time when a region of clear fluid appeared at the top of the pipe. Beyond this point, the filtering procedure described in the last section was employed.

In the special case when the suspension is neutrally buoyant ($\epsilon = 0$), the pipe flow is unidirectional and axisymmetric. An analytical solution of this reduced problem is available (Phillips *et al.* 1992) and was used in testing our code. Figure 2 shows the concentration profile in the radial direction

of the cross section for $\bar{\Phi} = 0.2$, where the solid curves represent our numerical results obtained with different number of elements and the dashed curve is the analytical solution. We see that the numerical results converge very rapidly and, even with a sparse mesh (only 32 elements and 147 nodes), the numerical curves almost coincide with the analytical profile, except near the centerline of the pipe where the analytical solution has the maximum value Φ_m so that the local viscosity is infinitely large, and where the concentration gradient is discontinuous. It is obvious that, in order to have the numerical results converge to the exact solution in the vicinity of this singular point, the local mesh resolution must be infinitely high.

We now present our predictions for the flow of suspensions containing heavy particles and compare them to the experimental results reported by Altobelli *et al.* (1991). Because the latter are given only in the form of color images and because our solutions using either [8] or [9] do not show qualitative differences, only numerical solutions using [8] will be presented hereafter for a qualitative comparison. Altobelli *et al.* (1991) used in their experiments Lubrabead particles of effective density 1.03 g/cm^3, mixed in a viscous oil of density 0.875 g/cm^3 and viscosity 3.84 P. The mean diameter of the particles was 0.762 mm and the inside diameter of the working pipe was 25.4 mm. Therefore, in our notation, $\epsilon \cong 0.2$ and $\lambda \cong 10^{-3}$. Figure 3 shows the contours of the computed concentration Φ and of the axial velocity u_3 for the sets of mean concentrations and flow rates which are in the ranges employed in the experiments. Specifically, the mean concentration $\bar{\Phi}$ in the three columns increases from 0.1 to 0.3 from left to right, and the flow rate Q is doubled row by row from bottom to top. We see that, under the action of gravity, a region of clear fluid ($\Phi \equiv 0$) appears at the top of the pipe in most cases, and that this region becomes smaller when the flow rate Q and/or the mean concentration $\bar{\Phi}$ increase, illustrating the enhancement of the resuspension with increasing of Q and $\bar{\Phi}$. We also see in figure 3 that the axial velocity profiles are blunt, especially when the mean concentration $\bar{\Phi}$ is high, and that the location of the maximum

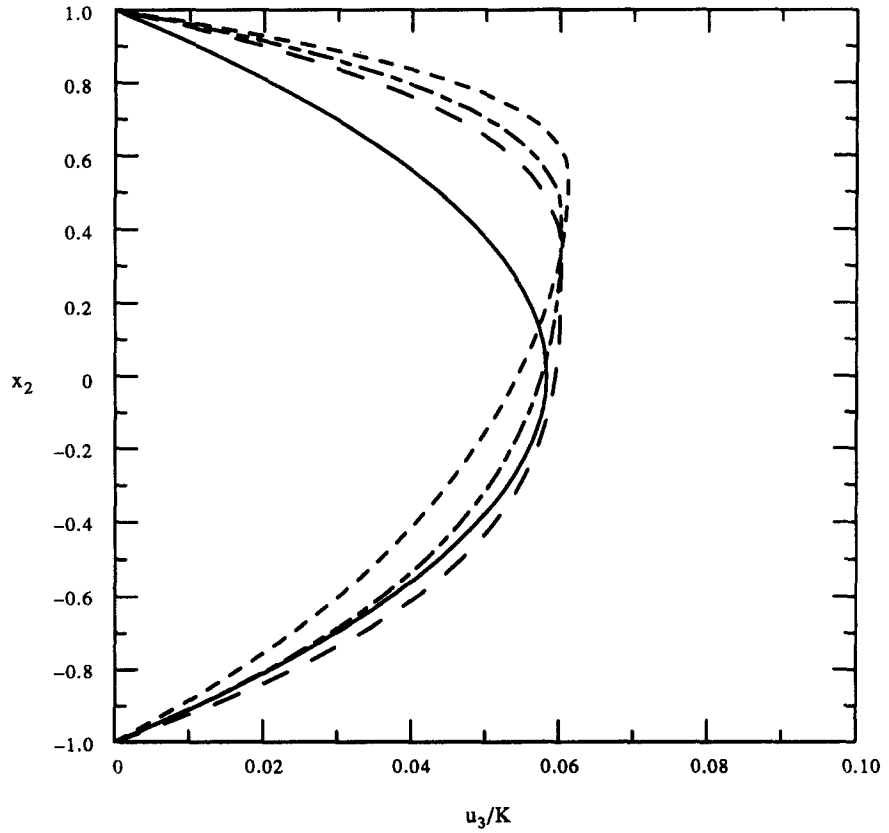

Figure 4. The profiles of the axial velocity, u_3/K, along the axis x_2 for the cases in column C of figure 3: C1, - - -; C2, —·—; C3, – – –. The solid curve represents the parabolic profile of a homogeneous suspension of $\Phi \equiv 0.3$.

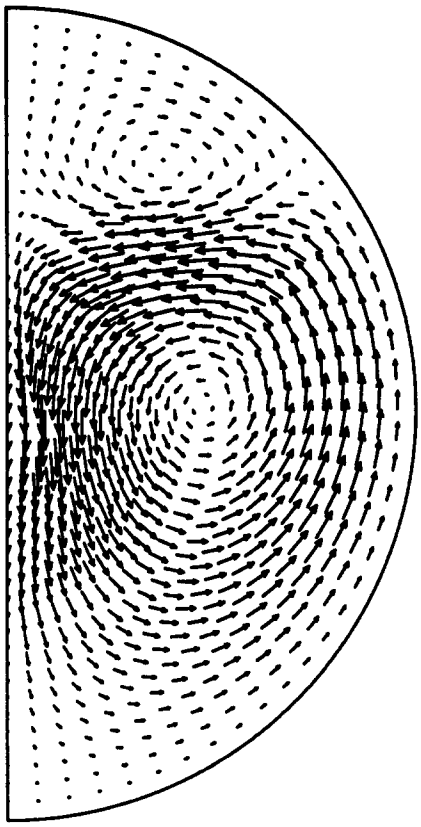

Figure 5. The velocity field of the secondary flow within the cross section for case B1 in figure 3.

axial velocity shifts above the centerline. These facts can be seen more clearly in figure 4, which depicts the profiles of the axial velocity along the vertical diameter of the cross section (the $x_1 = 0$ line) for $\bar{\Phi} = 0.3$ and where the parabolic profile of a homogeneous suspension with $\Phi = 0.3$ everywhere is also drawn for purposes of comparison.

It is especially encouraging that our results are also capable of predicting the experimental observation (Altobelli *et al.* 1991) that, when the mean concentration $\bar{\Phi}$ is high, the particles form a highly concentrated core, centered slightly above the pipe centerline and near the location of the maximum axial velocity. This concentrated core is illustrated by the dark-blue spots in column C of figure 3, where it is seen that, when the flow rate increases, the core becomes bigger and the corresponding maximum value of the concentration within the core also becomes slightly larger. The mechanism causing the formation of this core is that, when the particle concentration is high, the diffusion due to the shear-rate gradient is strong and creates a large upward flux of particles. On the other hand, when this part of the shear-induced diffusion is not strong enough to "support" the concentrated core, as in the case of low mean concentrations, the concentration decreases monotonically from the bottom to the top of the pipe. To test this hypothesis, we performed a simulation for the case C2 in figure 3 but without the diffusion term due to the shear-rate gradient (the second term of the right-hand side) of [13] and obtained a concentration distribution which was entirely different from that shown in figure 3, in that it decreases monotonically from the bottom to the top of the pipe.

By comparing our figure 3 to figure 6 in the paper by Altobelli *et al.* (1991), one can see that the predictions described above are in excellent agreement with the experimental results. A slight difference, though, exists, in that the predicted shape of the interface between the suspension and the clear fluid is concave rather than convex as shown by the experiment. This disagreement is primarily due to the convection resulting from the secondary flow, which, as illustrated by the vector field in figure 5, carries the particles up near the wall of the pipe and then down near the vertical plane of symmetry. In fact, if we artificially ignore this convective transport due to the

secondary flow, we indeed predict a convex interface, as demonstrated in figure 6 for the case of B1 of figure 3. This result and the fact that the suspension at the interface is very dilute and that, below the interface, the contours of the computed concentration are indeed convex, suggest, as one possibility, that the model may somehow underpredict the strength of the shear-induced diffusive flux when the local concentrations is very low.

Finally, we note that, as seen from the transport equation [13], the time scale, T, needed for suspension flows to reach a steady concentration distribution should be inversely proportional to λ, as pointed out by Nott & Brady (1994) in their analysis of pressure-driven suspension flows using Stokesian dynamics, and should also increase when the magnitude of the diffusion coefficients decreases. This last point was confirmed by our time dependent simulations. Specifically, for $\lambda = 10^{-3}$, we obtained steady solutions at about $T \sim 2000$ for $\bar{\Phi} = 0.3$ but only if $T > 3000$ for $\bar{\Phi} = 0.1$. This implies that, for measuring fully developed concentration profiles in a pipe flow, the inlet length in an experiment needs to be relatively longer when the feed suspension is dilute. This fact may account for the observation by Koh *et al.* (1994) that, for the case of flow of neutrally buoyant particles in a rectangular channel, the measured concentrations near the center of the channel were quantitatively lower than the corresponding values predicted theoretically, expecially when the feed concentration was low. These authors attributed this disagreement to the finite size of the particles which was not taken into account by the model used in their analysis which actually is very similar to ours. It is not obvious, however, that this effect can explain why their predicted concentration profiles matched their experimental data much better when the feed concentration was higher, e.g. when it was increased to $\bar{\Phi} = 0.3$.

Acknowledgements—This research was supported, in part, by a grant from the U.S. Department of Energy (Grant No. DE-F602-90-ER14139) and by the State of New York under its Einstein Chair Program.

REFERENCES

ACRIVOS, A., MAURI, R. & FAN, X. 1993 Shear-induced resuspension in a Couette device. *Int. J. Multiphase Flow* **19,** 797–802.

ALTOBELLI, S. A., GIVLER, R. C. & FUKUSHIMA, E. 1991 Velocity and concentration measurements of suspensions by nuclear magnetic resonance imaging. *J. Rheol.* **35,** 721–734.

BAKER, A. J. 1983 *Finite Element Computational Fluid Mechanics.* Hemisphere, New York.

BROOKS, A. N. & HUGHES, T. J. R. 1982 Streamline-upwind/Petrov–Galerkin formulations for convection dominated flows with particular emphasis on the incompressible Navier–Stokes equations. *Comput. Meth. Appl. Mech. Engng* **32,** 199–259.

HUGHES, T. J. R., LIU, W. K. & BROOKS, A. 1979 Finite element analysis of incompressible viscous flows by the penalty function formulation. *J. Comput. Phys.* **30,** 1–60.

KOH, C. J., HOOKHAM, P. A. & LEAL, L. G. 1994 An experimental investigation of concentrated suspension flows in a rectangular channel. *J. Fluid Mech.* **266,** 1–32.

KRIEGER, I. M. 1972 Rheology of monodisperse lattices. *Adv. Colloid Interface Sci.* **3,** 111–136.

LEE, R. L., GRESHO, P. M. & SANI, R. L. 1979 Smoothing techniques for certain primitive variable solutions of the Navier–Stokes equations. *Int. J. Numer. Meth. Engng* **14,** 1785–1804.

LEIGHTON, D. & ACRIVOS, A. 1986 Viscous resuspension. *Chem. Engng Sci.* **41,** 1377–1384.

LEIGHTON, D. & ACRIVOS, A. 1987 The shear-induced migration of particles in concentrated suspensions. *J. Fluid Mech.* **181,** 415–439.

NIR, A. & ACRIVOS, A. 1990 Sedimentation and sediment flow on inclinced surfaces. *J. Fluid Mech.* **212,** 139–153.

NOTT, P. R. & BRADY, J. F. 1994 Pressure-driven flow of suspensions: simulations and theory. *J. Fluid Mech.* In press.

PHILLIPS, R. J., ARMSTRONG, R. C. & BROWN, R. A. 1992 A constitutive equation for concentrated suspensions that accounts for shear-induced particle migration. *Phys. Fluids A* **4,** 30–40.

REDDY, J. N. 1984 *An Introduction to the Finite Element Method.* McGraw–Hill, New York.

SCHAFLINGER, U., ACRIVOS, A. & ZHANG, K. 1990 Viscous resuspension of a sediment within a laminar and stratified flow. *Int. J. Multiphase Flow* **16,** 567–578.

SINTON, S. W. & CHOW, A. W. 1991 NMR flow imaging of fluids and solid suspensions in Poiseuille flow. *J. Rheol.* **35,** 735–772.

USMANI, A. S., CROSS, J. T. & LEWIS, R. W. 1992 A finite element model for the simulations of mould filling in metal casting and the associated heat transfer. *Int. J. Numer. Meth. Engng* **35,** 787–806.

YILMAZER, U. & KALYON, D. M. 1989 Slip effects in capillary and parallel disk torsional flows of highly filled suspension. *J. Rheol.* **33,** 1197–1212.